Journal of Steroid Biochemistry and Molecular Biology 229 (2023) 106268

Contents lists available at ScienceDirect

Journal of Steroid Biochemistry and Molecular Biology

journal homepage: www.elsevier.com/locate/jsbmb

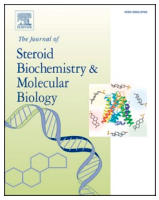

Comparative biochemical characterization of mammalian-derived CYP11A1s with cholesterol side-chain cleavage activities

Ruxin Liu [a,b], Yunjun Pan [a], Ning Wang [a,c], Dandan Tang [a], Vlada B. Urlacher [d], Shengying Li [a,b,*]

[a] State Key Laboratory of Microbial Technology, Shandong University, Qingdao, Shandong 266237, China
[b] Laboratory for Marine Biology and Biotechnology, Qingdao National Laboratory for Marine Science and Technology, Qingdao, Shandong 266237, China
[c] College of Life Sciences, Shandong Normal University, Jinan, Shandong 250014, China
[d] Institute of Biochemistry, Heinrich-Heine-University Düsseldorf, Universitätsstraße 1, Düsseldorf 40225, Germany

ARTICLE INFO

Keywords:
Cholesterol side-chain cleavage enzymes
CYP11A1
Pregnenolone
Steroids
Adrenodoxin
Adrenodoxin reductase
Cytochrome P450 enzymes

ABSTRACT

Steroid drugs, the second largest class of pharmaceuticals after antibiotics, have shown significant anti-inflammatory, anti-allergic, and endocrine-regulating effects. A group of cytochrome P450 enzymes, namely, CYP11A1 isoenzymes from different organisms are capable of converting cholesterol into pregnenolone, which is a pivotal reaction in both steroid metabolism and (bio)synthetic network of steroid products. However, the low activity of CYP11A1s greatly restricts the industrial application of these cholesterol side-chain cleavage enzymes. Herein, we investigate ten CYP11A1 enzymes of different origins and *in vitro* characterize two CYP11A1s with a relatively higher expression level from *Capra hircus* and *Sus scrofa*, together with the CYP11A1s from *Homo sapiens* and *Bos taurus* as references. Towards five selected sterol substrates with different side chain structures, *S. scrofa* CYP11A1 displays relatively higher activities. Through redox partners combination screening, we reveal the optimal redox partner pair of *S. scrofa* adrenodoxin and *C. hircus* adrenodoxin reductase. Moreover, the semi-rational mutagenesis for the active sites and substrate entrance channels of human and bovine CYP11A1s is performed based on comparative analysis of their crystal structures. The mutant m*Bt*CYP11A1-Q377A derived from mature *B. taurus* CYP11A1 shows a 1.46 times higher activity than the wild type enzyme. These results not only demonstrate the tunability of the highly conserved CYP11A1 isoenzymes, but also lay a foundation for the following engineering efforts on these industrially relevant P450 enzymes.

1. Introduction

Steroid drugs are widely used in the treatment of inflammation, allergic reactions, cardiovascular, endocrine and many other diseases, thus playing a central role in the pharmaceutical industry [1,2]. More than one million tons of steroid drugs are produced annually, and the total sales in 2016 were about 100 billion US dollars [2,3]. The traditional industrial production of steroids depends on semi-syntheses starting from diosgenin extracted from the plant turmeric as raw materials [4,5]. However, due to the disadvantages including turmeric price fluctuation and serious environmental pollution, the production of steroids has gradually been shifting to various microbial transformation approaches [3,6–8]. Despite the advantages of high regio- and stereoselectivity, mild reaction conditions, and environmental friendliness, microbial transformation still suffers from low conversion rates and productivity [4]. The *de novo* total biosynthesis of steroids provides a new means for their production. In 2003, the *de novo* total biosynthesis of hydrocortisone was firstly reported, establishing the proof-of-concept that the complex steroid biosynthetic pathway of higher eukaryotic organisms could be transferred to lower microorganisms such as *Saccharomyces cerevisiae* [9]. Nevertheless, due to the low activity of the enzymes involved in each step (especially several cytochrome P450 enzymes [10]) and the complexity of the whole metabolic process, the titer of hydrocortisone was only 11.5 mg/L. After more than ten years of optimization, the highest reported yield of *de novo* hydrocortisone biosynthesis was only 120 mg/L [11], which is far away from the requirement of industrial production.

The natural cholesterol side-chain cleavage P450 (P450scc) system consists of CYP11A1 localized to the inner mitochondrial membrane and its cognate redox partners (RPs) including adrenodoxin (Adx) located in the mitochondrial matrix and adrenodoxin reductase (AdR) associated with the inner mitochondrial membrane, which catalyzes the first and

* Corresponding author at: State Key Laboratory of Microbial Technology, Shandong University, Qingdao, Shandong 266237, China.
E-mail address: lishengying@sdu.edu.cn (S. Li).

https://doi.org/10.1016/j.jsbmb.2023.106268
Received 14 November 2022; Received in revised form 1 February 2023; Accepted 6 February 2023
Available online 9 February 2023

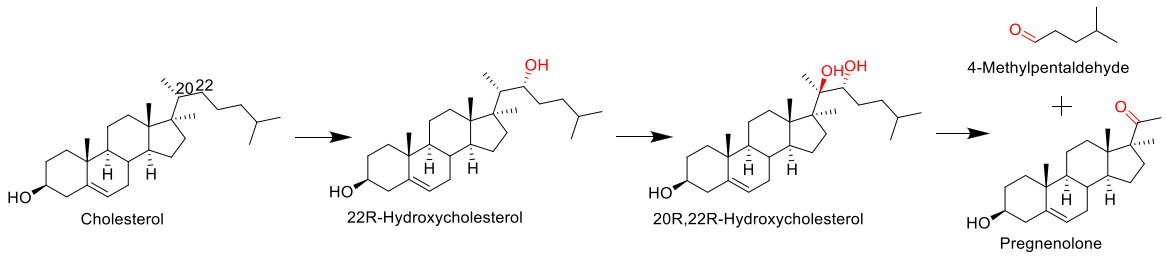

Fig. 1. The side-chain cleavage of cholesterol to pregnenolone by CYP11A1 with the redox partners Adx and AdR. The functional groups introduced by CYP11A1 are highlighted in red.

rate-limiting step in steroid hormone biosynthesis [12]. Specifically, CYP11A1 catalyzes a cascade of oxidative reactions including the initial C22-hydroxylation of cholesterol to give 22*R*-hydroxycholesterol tightly bound to the active site, further hydroxylation at C20 to yield 20*R*, 22*R*-dihydroxycholesterol, and the cleavage of the C20−C22 bond of 20*R*,22*R*-dihydroxycholesterol, giving rise to the final products pregnenolone and 4-methylpentanal (Fig. 1) [13]. Of note, pregnenolone is a key precursor/intermediate for the synthesis of progesterone and many other steroid drugs [14].

The heterologous expression of eukaryotic P450 usually faces multiple problems such as low expression level and difficulty in purification, which have been hindering the characterization and engineering of the membrane-bound CYP11A1s to a certain extent [15,16]. Up to now, only few CYP11A1s have been heterologously expressed in yeasts or *Escherichia coli* [17,18]. According to the previous reports, the highest yield of pregnenolone from cholesterol biotransformation by bovine CYP11A1 in *E. coli* was only 420 μg/L [18–20], while the production of pregnenolone in *Yarrowia lipolytica* reached 78 mg/L, representing the highest reported titer to date [7,17,21]. However, this titer/productivity is still too low for industrial application. Thus, it is crucial to identify new CYP11A1s or engineer CYP11A1 mutants in order to improve the activity.

In this study, we comparatively investigated four CYP11A1s *in vitro* including *Ch*CYP11A1 from *Capra hircus* (goat), *Ss*CYP11A1 from *Sus scrofa* (wild boar), *Tg*CYP11A1 from *Taeniopygia guttata* (zebra finches), and *Mm*CYP11A1 from *Mus musculus* (mouse) by using the well-studied *Hs*CYP11A1 from *Homo sapiens* (human) and *Bt*CYP11A1 from *Bos taurus* (ox) as references. Mammalian *Ch*CYP11A1, *Ss*CYP11A1, *Hs*CYP11A1 and *Bt*CYP11A1 with high expression levels were further biochemically characterized, including their substrate specificity and RP compatibility. Based on the protein sequence alignment and available crystal structures of CYP11A1s, semi-rational enzyme engineering was carried out and a CYP11A1 mutant with higher cholesterol side-chain cleavage activity *in vitro* was achieved.

2. Materials and methods

2.1. Materials

All sterol compounds were purchased from Aladdin (Shanghai, China) or Sigma Aldrich (St. Louris, MO, USA). All antibiotics were bought from Solarbio (Beijing, China). 2 × MultiF Seamless Assembly Mix was obtained from Abclonal (Wuhan, China). Plasmid Mini-prep Kit was provided by Tiangen (Beijing, China). The FlexiRun premixed gel solution for SDS-PAGE analysis was purchased from MDBio (Qingdao, China). The strains of *E. coli* BL21(DE3), JM109, and the plasmid vectors for protein expression of Fdx1499, FdR0978, m*Bt*Adx, m*Bt*AdR and RhFRED were preserved by our laboratory.

2.2. Phylogenetic tree

The CYP11A1 sequences were acquired by BLAST search for the Uniprot database with the query sequence of CYP11A1 from *Bos taurus* (Uniprot #: P00189). The sequences with identity greater than 45% were aligned using MUSCLE [22] and the phylogenetic tree was built using neighbor-jointing (NJ) method by MEGA 7.0 software. The phylogenetic tree was visualized using iTOL [23].

2.3. Molecular cloning and mutagenesis

The gene sequences encoding *Bt*CYP11A1 from *B. taurus* (P00189), *Ch*CYP11A1 from *Capra hircus* (P79153), *Ss*CYP11A1 from *Sus scrofa* (P10612), *Ec*CYP11A1 from *Equus caballus* (O46515), *Hs*CYP11A1 from *Homo sapiens* (P05108), *Mm*CYP11A1 from *Mus musculus* (Q9QZ82), *Oc*CYP11A1 from *Oryctolagus cuniculus* (Q28827), *Mg*CYP11A1 from *Meleagris gallopavo* (G1MUV6), *Tg*CYP11A1 from *Taeniopygia guttata* (Q6GVK8), *Dr*CYP11A1 from *Danio rerio* (Q7SYJ6), *Hs*Adx from *Homo sapiens* (P10109), *Ch*Adx from *C. hircus* (A0A452E7A8), *Ss*Adx from *S. scrofa* (P00258), *Hs*AdR from *H. sapiens* (P22570), *Ch*AdR from *C. hircus* (A0A452EV68), and *Ss*AdR from *S. scrofa* (F1RV70) were codon-optimized and synthesized by BGI•Write (Beijing, China). The mature form of CYP11A1s were sub-cloned into the pCWori vector with a *C*-terminal His_6-tag using 2 × MultiF Seamless Assembly Mix [24]. The genes encoding the mature forms of AdRs were sub-cloned into pET28a vector with a *C*-terminal His_6-tag. The genes encoding the truncated Adx (4−108)s with higher activities than wild type [25] were sub-cloned into pET28a vector with an *N*-terminal His_6-tag, and these truncated mutants will be presented as Adx for convenience. Mutational gene construction was achieved by site-directed mutagenesis *via* overlap extension PCR [26]. The primers used in this study are listed in Table S2. All constructs were confirmed by DNA sequencing at Sangon Biotech (Shanghai, China).

2.4. Protein expression and purification

For the expression of CYP11A1s and their mutants, the mature CYP11A1s were co-expressed with the *E. coli* molecular chaperone GroEL/ES in *E. coli* JM109 [27]. The strains were grown overnight at 37 °C with shaking at 220 rpm, and then used as seed cultures to inoculate (at a 1:100 ratio) Terrific Broth (TB) media. Cells were grown at 37 °C until OD_{600} reached 0.6–0.8. P450 expression was induced by the addition of isopropyl-*β*-D-1-thiogalactopyranoside (IPTG) (0.2 mM), *δ*-amino-levulinic acid (0.5 mM), rare salt solution [28], and arabinose (1.0 mM). The induced cultures were further incubated at 28 °C for 48 h with shaking at 150 rpm. The cells were harvested by centrifugation (1500 ×*g*) and then stored at − 80 °C for later use.

For the expression of Adxs and AdRs, the mature Adxs and AdRs were expressed in *E. coli* BL21(DE3). The strains were grown overnight at 37 °C with shaking at 220 rpm, and then inoculated into TB media with a ratio of 1:100. Cells were grown at 37 °C until OD_{600} reached 0.6–0.8. Protein expression was induced by the addition of IPTG (0.2 mM). The induced cultures were incubated at 18 °C for 20 h with shaking at 150 rpm. The cells were harvested by centrifugation (1500 ×*g*) and then stored at − 80 °C.

For purification of CYP11A1s, all the following steps were performed at 4 °C. Cell pellets were re-suspended in 50 mL lysis buffer (50 mM

potassium phosphate, 150 mM sodium chloride, 150 mM sodium acetate, 1% (*v/v*) Tween-20, 1% (*w/v*) sodium cholate, 10% (*v/v*) glycerol, and 10 mM imidazole, pH 7.4) through vortexing. The bacterial cells were disrupted by sonication on ice. Following removal of cell debris by centrifugation at 75,000 ×*g* for 30 min at 4 °C, to the cell lysate supernatants 1 mL Ni-NTA resin slurry was added and mixed gently for 1 h. The mixture was then loaded onto an empty column and washed with approximately 200 mL wash buffer (50 mM potassium phosphate, 150 mM sodium chloride, 150 mM sodium acetate, 1% (*v/v*) Tween-20, 1% (*w/v*) sodium cholate, 10% (*v/v*) glycerol, and 20 mM imidazole, pH 8.0) until no protein was eluted in flow-through. The His-tagged proteins were eluted with elution buffer (50 mM potassium phosphate, 150 mM sodium chloride, 150 mM sodium acetate, 1% (*v/v*) Tween-20, 1% (*w/v*) sodium cholate, 10% (*v/v*) glycerol, and 250 mM imidazole, pH 8.0). The eluents were concentrated with an Amicon Ultra centrifugal filter (30 kDa cutoff) and buffer-exchanged into storage buffer (50 mM potassium phosphate, 500 mM potassium chloride, 1% (*v/v*) Tween-20, 1% (*w/v*) sodium cholate, and 10% glycerol (*v/v*), pH 7.4). The final purified proteins were flash frozen by liquid nitrogen and stored at − 80 °C for later use. Carbon monoxide (CO) reduced difference spectra were used to determine the concentrations of purified CYP11A1s using the molar extinction coefficient of 91 $mM^{-1}cm^{-1}$ [29].

For purification of Adxs and AdRs, all the following steps were performed at 4 °C. The cell pellets were re-suspended in 50 mL lysis buffer (50 mM potassium phosphate, 300 mM potassium chloride, 10% glycerol, and 10 mM imidazole, pH 8.0), and then disrupted by ultrasonication. Cell-free lysates were prepared by centrifuging at 10,000 ×*g* for 1 h at 4 °C, to which 1 mL Ni–NTA resin slurry was added and mixed gently for 1 h. The mixture was loaded onto an empty column and washed with approximately 200 mL wash buffer (50 mM potassium phosphate, 300 mM potassium chloride, 10% (*v/v*) glycerol, 20 mM imidazole, pH 8.0) until no protein was eluted in flow-through. His-tagged proteins bound to Ni-NTA resin were eluted with 10 mL elution buffer (50 mM potassium phosphate, 300 mM potassium chloride, 10% glycerol, 250 mM imidazole, pH 8.0). The eluents were concentrated with an Amicon Ultra centrifugal filter (30 kDa cutoff for AdRs, and

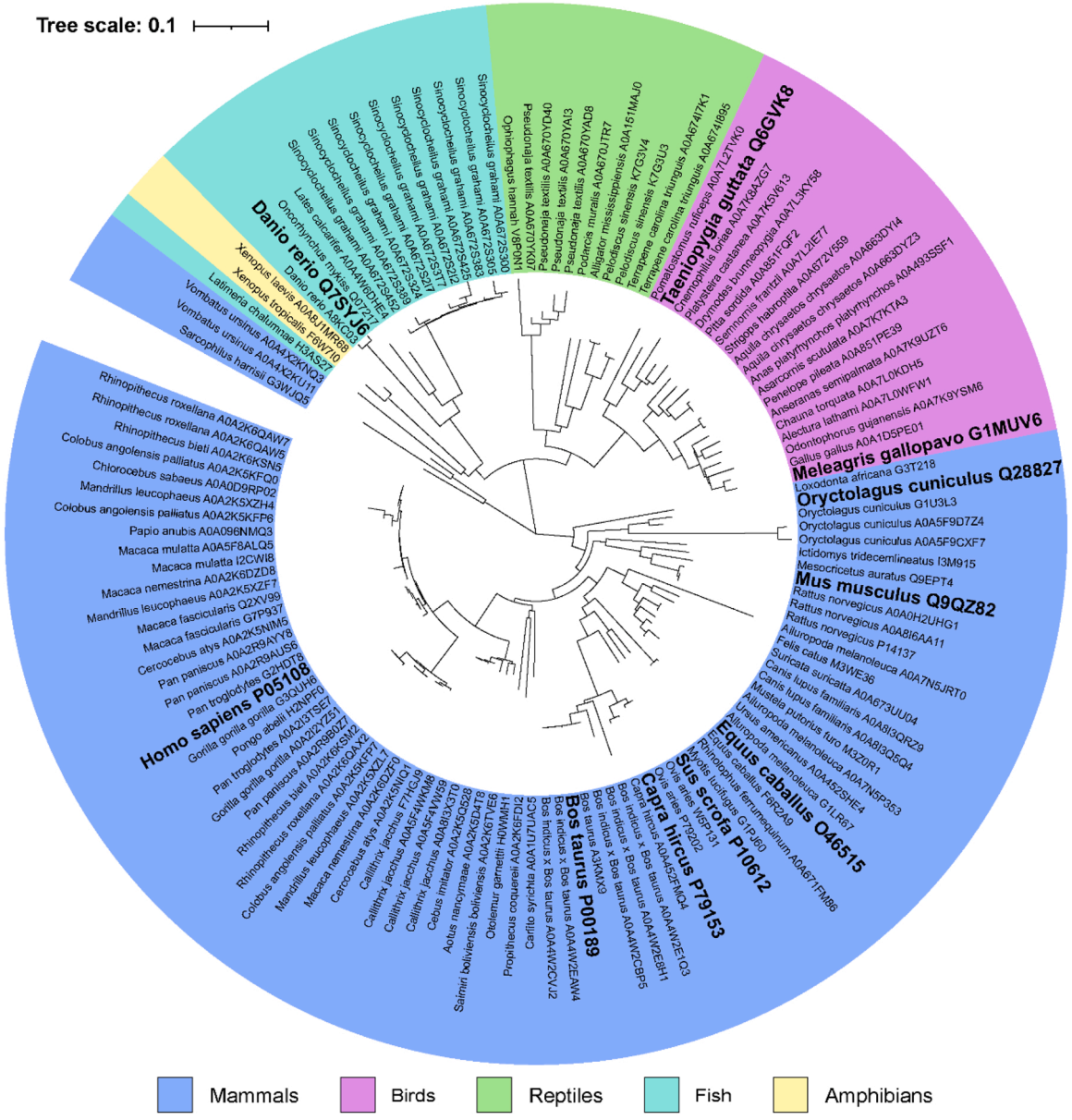

Fig. 2. Phylogenetic tree of CYP11A1 proteins. The phylogenetic tree was built from the protein sequences of CYP11A1 from *Bos taurus* (Uniprot #: P00189) and its homologous CYP11A1s with amino acid sequence homology greater than 45%, using the neighbor-joining method. The strain names denote the sources of the corresponding P450 enzymes.

10 kDa cutoff for Adxs) and buffer-exchanged into storage buffer (50 mM potassium phosphate, 10% glycerol, pH 7.4). The final purified proteins were flash frozen by liquid nitrogen and stored at − 80 °C. The final protein concentrations were calculated based on the molar extinction coefficients of $\varepsilon_{414} = 9.8\ mM^{-1}cm^{-1}$ for Adx [30] and $\varepsilon_{450} = 10.9\ mM^{-1}cm^{-1}$ for AdR [31].

2.5. In vitro enzymatic assay

The enzymatic reaction mixtures in 100 μl reaction buffer (pH 7.4, 50 mM potassium phosphate, 10% glycerol) consisted of 1 μM CYP11A1, 10 μM Adx, 5 μM AdR, 200 μM sterol substrate (prepared as 20 mM stock solutions in 45% (*w/v*) 2-hydroxypropyl-*β*-cyclodextrin), and an NADPH regeneration system comprised of 10 mM glucose-6-phosphate, 5 U glucose-6-phosphate dehydrogenase, and 2 mM NADPH. In the reactions using cholesterol, desmosterol, campesterol or *β*-sitosterol as substrates, the reactions were stopped by adding 10 μl 1 M HCl after incubation at 37 °C for 30 min, to which 50 μM of heptadecanoic acid (C17) as the internal standard was added, and the mixture was extracted by 120 μl ethyl acetate. The organic phase was analyzed by gas chromatography (GC). In the reactions using 7-dehydrocholesterol as substrate, the reactions were quenched by adding 200 μl methanol. Upon removal of the precipitations by high speed centrifugation (12,000 × *g*) for 10 min, the supernatants were analyzed with high-performance liquid chromatography (HPLC) or HPLC-high resolution mass spectrometry (HPLC-HRMS). All enzymatic reactions were carried out in triplicate, and statistical analyses were performed using the Student's *t* test or ANOVA.

2.6. Homology modeling

The 3D structure of m*Bt*CYP11A1-Q377A was generated by using the homology modeling function of SWISS-MODEL [32], and the crystal structure of m*Bt*CYP11A1 (PDB ID code: 3MZS) was used as the template.

2.7. Steady-state kinetic analysis

In a standard kinetic assay, 0.5–1 μM CYP11A1, 10 μM Adx, 5 μM AdR, and 20–200 μM cholesterol were pre-incubated in 50 μl reaction system at 37 °C for 5 min. 2 mM NADPH was added into the system for reaction initiation. The reaction was quenched at 0, 1, and 3 min by adding 10% (*v/v*) of 1 M HCl. Sample extraction and analysis were performed the same as above for GC analysis. Initial rates were calculated in terms of the substrate consumption by enzymes. Kinetic analyses were performed using OriginPro 2021 program.

2.8. Analytical methods

The Agilent 7890B gas chromatograph equipped with a capillary column HP-5 (Agilent Technologies, Santa Clara, CA, USA; cross-linked polyethylene glycerol, i.d. 0.25 μm film thickness, 30 m by 0.32 mm) was used for all GC analyses. The flow rate of helium was set to 1 mL/min. The oven program was set initially at 70 °C for 1 min, then increased to 250 °C by the rate of 20 °C per min and held for 2 min, and finally increased to 280 °C by the rate of 15 °C per min and held for 15 min. The injecting temperature was set to 300 °C with 1 μl injection volume. HPLC analyses were carried out on a Thermo Ultimate 3000 instrument. HPLC-HRMS analyses were performed on a Bruker impact HD High Resolution Q-TOF mass spectrometry. All HPLC and HPLC-HRMS analyses were performed using a Triart C18 column under a linear mobile phase gradient ranging from 64% (*v/v*) methanol/H_2O to 100% methanol.

2.9. Molecular docking analysis

The molecular structures of cholesterol, 7-dehydrocholesterol, desmosterol, campesterol, and *β*-sitosterol were generated using Chembio3D Ultra 14.0 followed by energy minimization. Substrates were docked into the structure of m*Bt*CYP11A1 (PDB ID code: 3MZS) using Autodock 4.2 [33] equipped with ADT after all waters were removed. All side chains were set as rigid body and grid spacing was set to 0.5 Å. Other parameters retained their default values. The top 10 lowest energy docking poses of the substrates from 2500,000 searching results were selected, among which the ideal catalytic conformations were chosen for further analysis.

3. Results

3.1. Selection of CYP11A1 based on genome mining

Explosive genome sequencing data has led to disclosure of a large number of CYP11A1 genes. However, only three CYP11A1 isoenzymes from *Homo sapiens* (Uniprot #: P05108), *Bos taurus* (Uniprot #: P00189), and *Bufo gargarizans* (GenBank accession #: XP_044139300) have been characterized *in vitro* [34–40]. To explore more cytochrome P450 enzymes with the cholesterol side-chain cleavage activity, we BLAST searched the CYP11A1s in the Uniprot database using *Bt*CYP11A1 (Uniprot #: P00189) as a sequence probe and constructed a phylogenetic tree for the sequence homologues with the protein sequence identity greater than 45% (Fig. 2). The phylogenetic tree shows that all hit CYP11A1 sequences are derived from vertebrates, of which mammals account for the highest proportion of 62%, followed by birds, accounting for 15%. *Vombatus ursinus* (wombat) and *Sarcophilus harrisii* (Tasmanian devil) are relatively ancient mammals, whose CYP11A1s appear as independent clades on the evolutionary tree. *Latimeria chalumnae*, as one of the oldest fishes and the extant coelacanths, whose CYP11A1 is evolutionarily closer to those of lungfish and tetrapods, is not on the same branch of fishes. These results suggest that CYP11A1s might be an excellent evolutionary indicator for vertebrates.

On the basis of this phylogenetic analysis, we selected ten CYP11A1s with different levels of homology and origins (Fig. 2) for the following biochemical studies, among which seven were derived from different mammals: *Bt*CYP11A1 (P00189, 100% identity), *Ch*CYP11A1 from *Capra hircus* (P79153, 95% identity), *Ss*CYP11A1 from *Sus scrofa* (P10612, 84% identity), *Ec*CYP11A1 from *Equus caballus* (O46515, 75% identity), *Hs*CYP11A1 (P05108, 72.9%), *Mm*CYP11A1 (Q9QZ82, 67.8% identity), and *Oc*CYP11A1 from *Oryctolagus cuniculus* (Q28827, 68.8% identity); two from birds: *Mg*CYP11A1 from *Meleagris gallopavo* (G1MUV6, 53.1% identity), and *Tg*CYP11A1 from *Taeniopygia guttata* (Q6GVK8, 49.5% identity); and one from fish: *Dr*CYP11A1 from *Danio rerio* (Q7SYJ6, 45.4% identity).

3.2. Determination of the substrate specificity of selected CYP11A1s

Considering that *E. coli* itself does not express any endogenous P450 protein which avoids the background P450 interference for CYP11A1 activity detection and that there has been not a few precedents for successful heterologous expression of eukaryotic P450s in *E. coli*, we chose *E. coli* as the heterologous expression host for the above-selected CYP11A1s. To optimize expression of the eukaryotic membrane-associated CYP11A1s in *E. coli*, the ten CYP11A1 genes were synthesized with codon optimization for the prokaryotic host and the *N*-terminal mitochondrial targeting sequences were removed (Fig. S1). Furthermore, in order to increase the expression level of CYP11A1, the molecular chaperones GroEL/GroES were co-expressed to assist CYP11A1 for proper protein folding [27]. After expression of these mature CYP11A1 proteins in *E. coli* JM109, the formation of different levels of pregnenolone from cholesterol was detected in reactions with six out of the ten cell lysates (Fig. S4). Among the six active CYP11A1s,

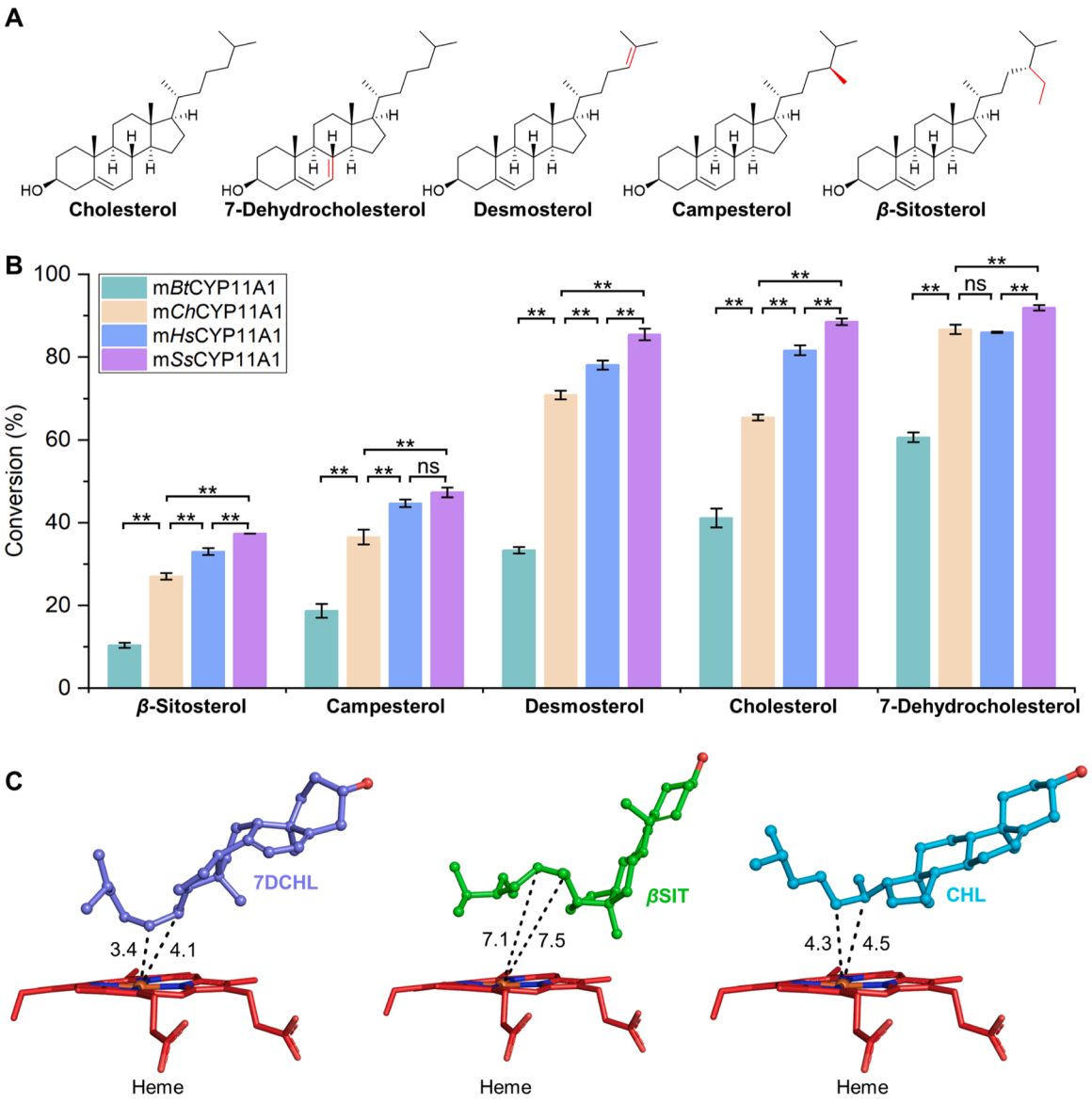

Fig. 3. The activities of four CYP11A1s towards different substrates. A, The structures of the sterol substrates used in this study. The structural differences from cholesterol are highlighted in red. B, The side-chain cleavage activities of four CYP11A1s towards each certain substrate. The comparisons of the side-chain cleavage activities of each individual CYP11A1 of different origin towards five sterol substrates are shown in Fig. S7. In a standard 100 µl reaction, 1 µM enzyme, 10 µM m*Bt*Adx, 5 µM m*Bt*AdR, 200 µM substrate, and 2 mM NADPH were co-incubated at 37 °C for 30 min. Results are shown as mean ± SD (n = 3). **C**, Docking analysis of 7-dehydrocholesterol (7DCHL) and *β*-sitosterol (*β*SIT) into m*Hs*CYP11A1 with the co-crystal structure of cholesterol (CHL) and m*Hs*CYP11A1 as a reference. 7DCHL, *β*SIT, and CHL are shown in slate, green, and cyan, respectively. Statistical analysis was performed using the one-way ANOVA with Bonferroni's test for *post hoc* analysis (*P < 0.05, **P < 0.01, ns: P > 0.05, not significant).

due to the very low expression levels (Table S1) of m*Mm*CYP11A1 (m: mature) and m*Tg*CYP11A1, four P450 enzymes including m*Ch*CYP11A1, m*Ss*CYP11A1, m*Bt*CYP11A1 and m*Hs*CYP11A1 were selected for the following studies. Following the previously established procedure, which utilized sodium cholate as the detergent to solubilize the membrane-bound m*Bt*CYP11A1 [41], we successfully purified these four proteins, which all showed the characteristic absorption peaks in their carbon monoxide (CO) reduced differential absorption spectra, indicating that they were functional P450 enzymes (Fig. S5) [42].

To investigate the substrate specificity of these CYP11A1s, we comparatively determined their catalytic activities *in vitro* against five different sterol substrates, including *β*-sitosterol, campesterol, desmosterol, cholesterol, and 7-dehydrocholesterol, using purified P450 enzymes and the bovine RP proteins m*Bt*Adx and m*Bt*AdR (Fig. 3A). The results showed that all four mCYP11A1s were capable of catalyzing the side-chain cleavage reactions of these sterol substrates to generate pregnenolone or 7-dehydropregnenolone (identified by HRMS, Fig. S6) (Figs. 3B and S7). As results, m*Ss*CYP11A1 exhibited higher activities toward all tested substrates than m*Ch*CYP11A1 (Fig. 3B), and the conversion ratios for *β*-sitosterol, campesterol, desmosterol, cholesterol, and 7-dehydrocholesterol were 37.4%, 47.3%, 85.5%, 88.5%, and 90.3%, respectively. This *in vitro* result is consistent with the previously determined *in vivo* activity of m*Ss*CYP11A1 against campesterol in *Yarrowia lipolytica* [17]. Surprisingly, m*Bt*CYP11A1 gave the lowest conversion ratios for all the substrates, even though it was paired with the cognate RPs. For all four CYP11A1s, 7-dehydrocholesterol and *β*-sitosterol turned out to be the most favorable and unfavorable substrates, respectively.

To rationalize the different catalytic performance of CYP11A1 towards the five structurally similar substrates, we docked each individual

substrate into the active site of m*Hs*CYP11A1 (PDB ID code: 3N9Y) to analyze the structure-function relationship using Autodock 4.2 [33]. The docking result of 7-dehydrocholesterol revealed that the C22 is closer (3.4 Å) to the heme iron than the C22 of cholesterol (4.3 Å), which at least partly explains the preference of m*Hs*CYP11A1 for 7-dehydrocholesterol (Fig. 3 C). Modeling of desmosterol, campesterol and β-sitosterol showed a trend that with increasing side chain modification (unsaturation in desmosterol, C24-methylation in campesterol, and C24-ethylation in β-sitosterol), the C22-to-iron distance (5.4 Å, 5.5 Å, and 7.1 Å, respectively) increases (Fig. S8). Moreover, the catalytic activity of all the CYP11A1s for these three substrates decreased with the increasing distance between the substrate C22 and the heme-iron reactive center. In all docking results, the distance between the substrate C22 and heme-iron is consistently closer than that of C20, indicating that C22 is preferentially hydroxylated; this is consistent with the previous report [13,43].

3.3. Evaluation of the supporting activities of RPs

According to the classification of P450 enzymes based on RP systems, CYP11A1 located in the inner mitochondrial membrane belongs to Class I P450 [15,16]. Its cognate RPs are Adx and AdR that are also located inside mitochondria, which are responsible for sequentially transferring two electrons originated from NADPH to the heme-iron reaction center of CYP11A1, so as to activate O_2 to complete the oxidative cleavage reaction [44–46]. Since appropriate RPs are critical for the catalytic activity of P450 enzymes, we sought to reveal the optimal RPs by activity screening especially considering that in some cases the heterologous RPs may be more active than native ones [17,44]. For example, it was reported that the activity of CYP109D1 from *Sorangium cellulosum* So ce56 in combination with *Bt*Adx/*Bt*AdR *in vitro* increased 3–5 folds compared with the use of endogenous RPs [47]. The production of pregnenolone increased 17.5 folds by *in vivo* combination screening of nine CYP11A1s of different sources and four different Adx/AdR pairs in *Yarrowia lipolytica* [17]. Previous studies also showed that the RPs from *S. cellulosum* and *Anemarrhena asphodeloides* could support the side-chain cleavage activity of CYP11A1 [40,48].

Encouraged by these results, we first tested the supporting activity of the cyanobacterium *Synechococcus elongates* derived Fdx1499/FdR0978 [44,49] and the *Rhodococcus sp.* NCIMB 9784 derived RhFRED [50] as surrogate RPs for m*Hs*CYP11A1 [51]. As results, RhFRED failed to support the cholesterol side-chain activity of m*Hs*CYP11A1 *in vitro*, and Fdx1499/FdR0978 resulted in a lower activity than with m*Bt*Adx/m*Bt*AdR giving a relative activity of 10.3% (Fig. S9), demonstrating the possibility that the bacterial-derived RPs could act as a substitute for the eukaryotic mitochondria-derived RPs. In addition, in the cross-combinations of m*Hs*CYP11A1/Fdx1499/m*Bt*AdR and m*Hs*CYP11A1/m*Bt*Adx/FdR0978, the reaction products were also detected. The relative activity by m*Hs*CYP11A1/m*Bt*Adx/FdR0978 (63.8%) was much higher than that of m*Hs*CYP11A1/Fdx1499/FdR0978 (10.3%), while m*Hs*CYP11A1/Fdx1499/m*Bt*AdR (4.7%) gave a much lower conversion than m*Hs*CYP11A1/m*Bt*Adx/m*Bt*AdR (100%), clearly indicating that Adx is more important than AdR for the P450-supporting activity since Adx rather than AdR directly interacts with CYP11A1. In conclusion, although Fdx1499/FdR0978 have been shown as extraordinary RP proteins [44,52,53], CYP11A1 seems to prefer the mitochondrial Adx/AdR that might have co-evolved with CYP11A1 for a long history. In addition, inspired by the interesting finding that some ancestral CYP11A1 enzymes show tolerance to hydrogen peroxide [41], we also determined whether H_2O_2 could replace RPs to support the m*Hs*CYP11A1 catalyzed reactions; however, no activity was detected when H_2O_2 acted as the sole electron and oxygen donor.

Next, we turned to examine the CYP11A1-supporting activities of different combinations of mitochondrial Adx and AdR. Specifically, m*Ch*Adx (Uniprot #: A0A452E7A8) and m*Ch*AdR (Uniprot #: A0A452EV68) from *C. hircus*, m*Hs*Adx (Uniprot #: P10109) and m*Hs*AdR (Uniprot #: P22570) from *H. sapiens*, and m*Ss*Adx (Uniprot #: P00258) and m*Ss*AdR (Uniprot #: F1RV70) from *S. scrofa* were heterologously expressed in *E. coli* BL21(DE3) after codon-optimization and purified to homogeneity (Figs. S2-S3, S10). Unsurprisingly, the four pairs of Adx/AdR of common origin were able to cross-support the catalytic activities of four CYP11A1s from different sources. The human, bovine and goat RPs only showed little differences in supporting the four tested CYP11A1s (Table 1). Furthermore, when we cross-combined Adx and AdR of different sources, attempting to obtain an optimal RP combination for m*Hs*CYP11A1, we found that the combination of m*Ss*Adx/m*Ch*AdR gave a 1.1-fold increased activity relative to the initially used m*Bt*Adx/m*Bt*AdR (Table 2). This result indicates that the screening of RP combinations has certain potential in improving the catalytic activity of a P450 system, as we reported previously [44,49].

Table 1
Cholesterol conversion ratios of four CYP11A1s partnered by different Adx/AdR pairs from the same origin.

CYP11A1s	Redox partners	Conversion (%)
m*Bt*CYP11A1	m*Bt*Adx/m*Bt*AdR	69.8 ± 1.3
	m*Hs*Adx/m*Hs*AdR	67.6 ± 1.5 ^{ns}
	m*Ch*Adx/m*Ch*AdR	65.6 ± 1.4 ^{ns}
	m*Ss*Adx/m*Ss*AdR	60.4 ± 0.8 **
m*Hs*CYP11A1	m*Bt*Adx/m*Bt*AdR	83.5 ± 1.9
	m*Hs*Adx/m*Hs*AdR	89.4 ± 2.1 ^{ns}
	m*Ch*Adx/m*Ch*AdR	90.9 ± 0.8 *
	m*Ss*Adx/m*Ss*AdR	87.5 ± 1.9 ^{ns}
m*Ch*CYP11A1	m*Bt*Adx/m*Bt*AdR	83.3 ± 1.9
	m*Hs*Adx/m*Hs*AdR	82.8 ± 0.6 ^{ns}
	m*Ch*Adx/m*Ch*AdR	82.6 ± 1.6 ^{ns}
	m*Ss*Adx/m*Ss*AdR	68.4 ± 1.3 **
m*Ss*CYP11A1	m*Bt*Adx/m*Bt*AdR	93.2 ± 0.5
	m*Hs*Adx/m*Hs*AdR	92.5 ± 1.7 ^{ns}
	m*Ch*Adx/m*Ch*AdR	90.9 ± 2.4 ^{ns}
	m*Ss*Adx/m*Ss*AdR	90.4 ± 1.8 ^{ns}

All experiments were independently repeated for three times. Statistical analysis was performed using the Student's *t* test (two-tailed; *P < 0.05, **P < 0.01, ns: P > 0.05, not significant; two-sample unequal variance).

Table 2
Relative activities of m*Hs*CYP11A1 when partnered by different intra- and interspecies combinations of Adx and AdR.

Redox partner combinations	Relative activity (%)
m*Bt*Adx/m*Bt*AdR	100
m*Hs*Adx/m*Hs*AdR	107.1 ± 2.1 ^{ns}
m*Ch*Adx/m*Ch*AdR	108.9 ± 0.8 *
m*Ss*Adx/m*Ss*AdR	104.7 ± 1.9 ^{ns}
m*Bt*Adx/m*Hs*AdR	110.7 ± 0.9 **
m*Bt*Adx/m*Ch*AdR	105.7 ± 1.3 *
m*Bt*Adx/m*Ss*AdR	105.8 ± 2.2 ^{ns}
m*Hs*Adx/m*Bt*AdR	101.6 ± 3.4 ^{ns}
m*Hs*Adx/m*Ch*AdR	109.5 ± 0.9 **
m*Hs*Adx/m*Ss*AdR	102.9 ± 3.2 ^{ns}
m*Ch*Adx/m*Bt*AdR	107.2 ± 2.6 ^{ns}
m*Ch*Adx/m*Hs*AdR	107.5 ± 1.9 *
m*Ch*Adx/m*Ss*AdR	107.3 ± 2.3 ^{ns}
m*Ss*Adx/m*Bt*AdR	105.2 ± 1.9 ^{ns}
m*Ss*Adx/m*Hs*AdR	111.1 ± 0.3 **
m*Ss*Adx/m*Ch*AdR	110.7 ± 1.4 **

All experiments were independently repeated for three times. Statistical analysis was performed using the Student's *t* test (two-tailed; *P < 0.05, **P < 0.01, ns: P > 0.05, not significant; two-sample unequal variance).

3.4. Site-directed mutagenesis

Although the crystal structures of human and bovine CYP11A1s have been solved, to our best knowledge, there has been only one mutational analysis report on three active site residues in m*Bt*CYP11A1 [54], and a limited number of studies on CYP11A1 enzyme engineering [55–57]. To

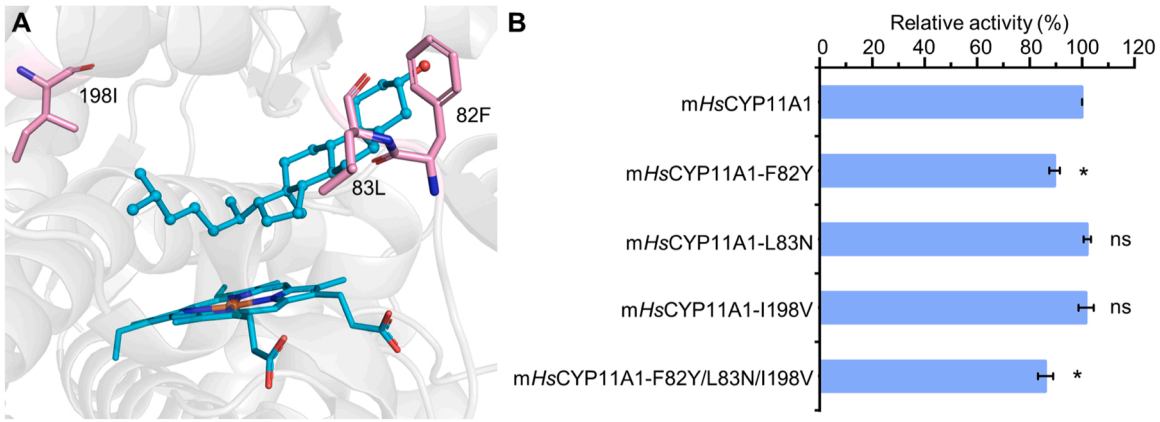

Fig. 4. Comparison of the relative activities of m*Hs*CYP11A1 and its mutants towards cholesterol. A, The selected mutational sites. B, The relative activities of m*Hs*CYP11A1 and its mutants. The activity of m*Hs*CYP11A1 towards cholesterol (conversion ratio: 81.6%) is assigned as 100%. In a standard 100 μl reaction, 1 μM P450 enzyme, 10 μM m*Ss*Adx, 5 μM m*Ch*AdR, 200 μM substrate, and 2 mM NADPH were co-incubated at 37 °C for 30 min. Results are shown as mean ± SD (n = 3). Statistical analysis was performed using the Student's *t* test (two-tailed; *P < 0.05, **P < 0.01, ns: P > 0.05, not significant; two-sample unequal variance).

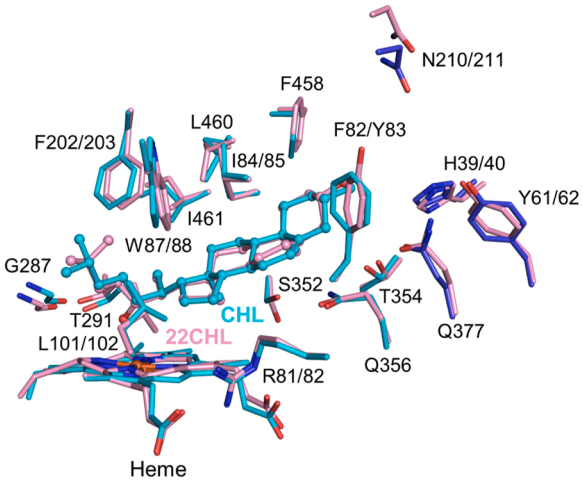

Fig. 5. Comparison of the active sites of m*Hs*CYP11A1 and m*Bt*CYP11A1. The residues of active site and substrate entrance channel in m*Hs*CYP11A1 (PDB ID code: 3N9Y) are labelled in cyan and blue, respectively. Cholesterol (CHL) and heme are in cyan. The residues, 22R-hydroxycholesterol (22CHL) and heme of m*Bt*CYP11A1 (PDB ID code: 3MZS) are shown in pink.

improve the catalytic activity of CYP11A1, we decided to perform semi-rational engineering for these cholesterol side chain cleavage enzymes. First, through protein sequence alignment, we found that the active sites of the four CYP11A1s are highly conserved, with only three different amino acids (*i.e.*, the 82nd, 83rd, and 198th amino acids) out of the 28 amino acids within 6 Å distance from the substrate (Fig. S11). Second, we singly mutated F82, L83 and I198 in m*Hs*CYP11A1 into the corresponding amino acids Y, N and V in m*Ss*CYP11A1 (with higher activity, Fig. 4), and also constructed a triple mutant F82Y/L83N/I198V of m*Hs*CYP11A1 (Fig. S12A). According to the activity comparison of these four mutants (Fig. 4), the mutant enzymes m*Hs*CYP11A1-L83N and m*Hs*CYP11A1-I198V showed marginally higher activities than m*Hs*CYP11A1 with the relative activities of 102.0% and 101.5%, respectively. The triple mutant had the lowest activity with a relative activity of 86.1%. These results suggest that the activity of CYP11A1 might be related to the three varied amino acid residues.

Next, based on the crystal structure of m*Hs*CYP11A1, we selected a total of 18 residues located within the active site or at the substrate entrance channel, and performed alanine scanning in order to find some mutational hot spots. However, only eight mutant enzymes could be substantially purified and quantified (Fig. S12B) since the soluble fractions of the remaining ten proteins were extremely low. To address this issue, we turned to re-construct these ten mutants based on m*Bt*CYP11A1 for two reasons: 1) the protein sequences of m*Hs*CYP11A1 and m*Bt*CYP11A1 are highly similar to each other (with a homology of 72.9%), and their active pockets have only one amino acid difference (Fig. 5); and 2) the expression level of m*Bt*CYP11A1 in *E. coli* was found to be significantly higher than that of m*Hs*CYP11A1. As expected, we successfully expressed and purified the ten m*Bt*CYP11A1 mutants (Fig. S12C) as a complement to the eight m*Hs*CYP11A1 mutants. With regard to the catalytic activities of these mutant enzymes, none of m*Hs*CYP11A1 mutants gave a higher activity than the wild type enzyme, and m*Hs*CYP11A1-F202A totally lost the catalytic ability. By contrast, the catalytic activity of m*Bt*CYP11A1-Q377A was 46.0% higher than that of m*Bt*CYP11A1, while the activities of other mutants decreased to varying degrees, among which m*Bt*CYP11A1-W88A was a dead mutant (Fig. 6). The inactivity of m*Hs*CYP11A1-F202A and m*Bt*CYP11A1-W88A suggests that the two sites located around the side chain of cholesterol should be functionally essential and evolutionarily conserved.

Motivated by the improved activity of m*Bt*CYP11A1-Q377A, we further constructed Q377A mutants of m*Ss*CYP11A1 and m*Ch*CYP11A1. Unexpectedly, the catalytic activity of m*Ss*CYP11A1 and m*Ch*CYP11A1 Q377A mutants for cholesterol did not increase, but decreased. These results indicate that Q377 may be a hot spot specific to m*Bt*CYP11A1, and the plasticity of m*Bt*CYP11A1 is stronger than that of CYP11A1s with better activities. Collectively, we suggest that Q377 located in the m*Bt*CYP11A1 substrate entrance channel might be a hot spot for future enzyme engineering and mechanistic investigation, and m*Bt*CYP11A1 Q377A can be used as a parental enzyme for CYP11A1 retrofit design.

Rational and semi-rational protein engineering mainly focuses on the active site of enzyme, while the residues located at the substrate entrance channel have also received increasing attention in recent years [58–60]. To further shed some light on the reason for the improved catalytic activity of m*Bt*CYP11A1-Q377A from the perspective of structure-function relationship, we compared the diameters of the substrate entrance channels of m*Bt*CYP11A1 (real crystal structure) and m*Bt*CYP11A1-Q377A (modelled structure using SWISS-MODEL [32]). The distance of m*Bt*CYP11A1 from N210 to Q377 is 9.6 Å, while the corresponding distance of m*Bt*CYP11A1-Q377A from N210 to A377 is increased to 12.9 Å (Fig. 6C, D). The larger substrate entrance may make the substrate enter and/or the product leave the active site more easily [61,62]. In addition, the replacement of the polar side chain of Q377 by the non-polar side chain of alanine would enhance the hydrophobicity of the substrate entrance channel, thus favoring the traffic of the highly hydrophobic sterol substrates. To further evaluate the catalytic

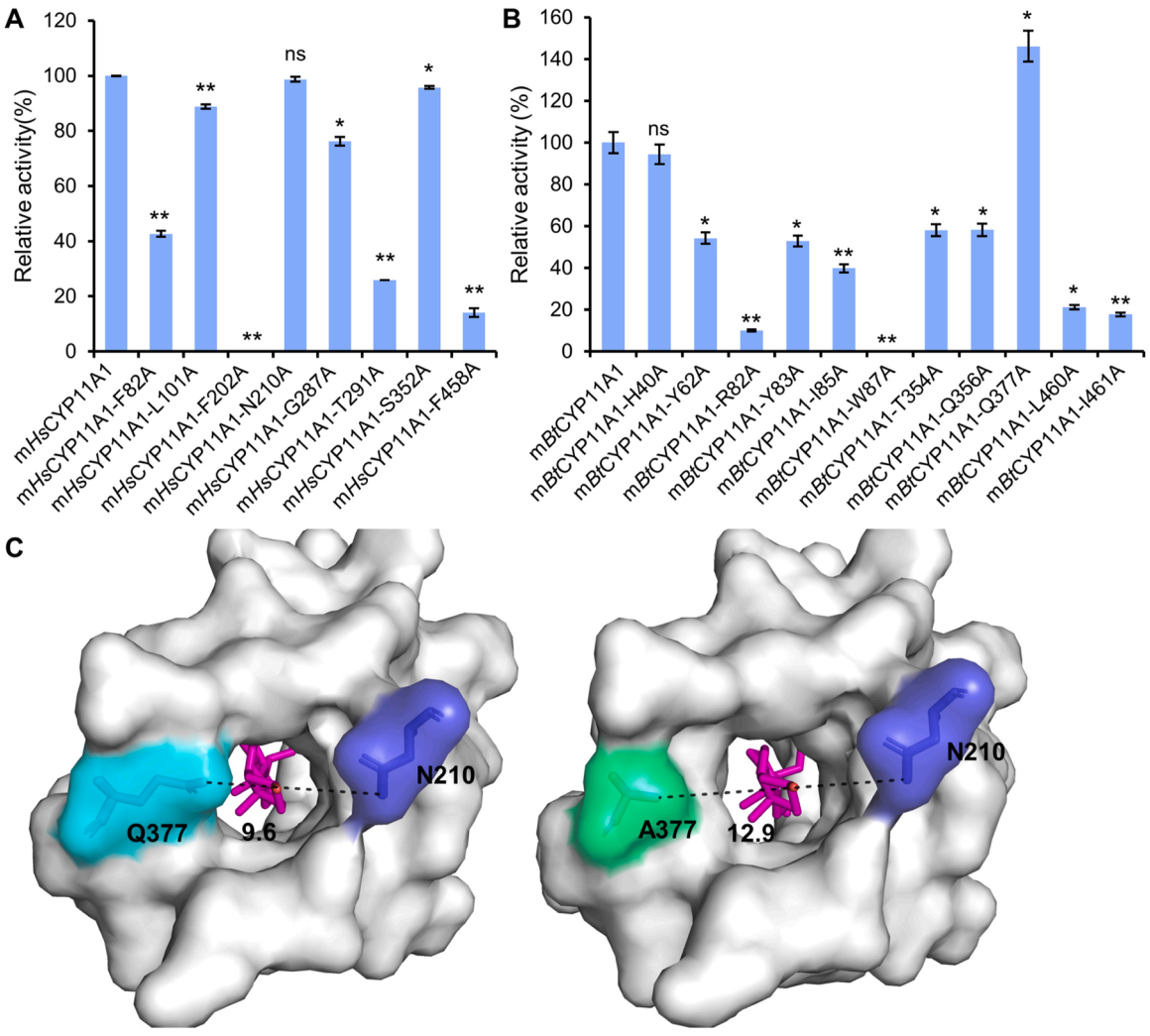

Fig. 6. Comparison of the relative cholesterol side-chain cleavage activities of m*Hs*CYP11A1, m*Bt*CYP11A1, and their corresponding mutants. A, The relative activities of m*Hs*CYP11A1 and its mutants, data are scaled to the corresponding activity of m*Hs*CYP11A1 (the conversion ratio of 83.5% is assigned as 100% relative activity). B, The relative activities of m*Bt*CYP11A1 and its mutants, data are scaled to the corresponding activity of m*Bt*CYP11A1 (the conversion ratio of 41.1% is assigned as 100% relative activity). C, Comparison of the substrate entrance channels of m*Bt*CYP11A1 and m*Bt*CYP11A1-Q377A. The distances from N210 (blue) to Q377 (cyan) and to A377 (green) are shown by dashed lines in angstrom. Cholesterol is shown in magenta. Statistical analysis was performed using the Student's *t* test (two-tailed; *P < 0.05, **P < 0.01, ns: P > 0.05, not significant; two-sample unequal variance).

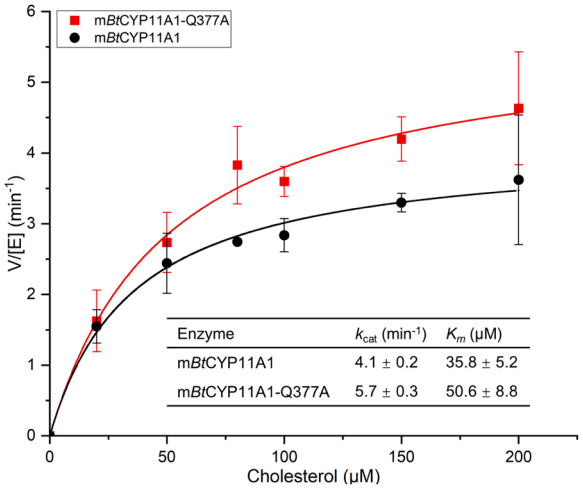

Fig. 7. The steady-state kinetic curves of m*Bt*CYP11A1 and m*Bt*CYP11A1-Q377A towards cholesterol when supported by m*Bt*Adx/m*Bt*AdR.

properties of m*Bt*CYP11A1-Q377A, we determined the steady-state kinetic parameters using m*Bt*Adx and m*Bt*AdR as RPs. Compared with the wild type m*Bt*CYP11A1, whose k_{cat} and K_m are consistent with the previous report [63], the apparent k_{cat} value of m*Bt*CYP11A1-Q377A increased by 1.4 times, but the substrate-binding affinity was lower with a 1.4-fold higher apparent K_m value. Overall, the k_{cat}/K_m values of m*Bt*CYP11A1 and m*Bt*CYP11A1-Q377A were very close to each other. However, at the substrate concentration of 200 μM used for the enzymatic assays (Fig. 6B), the velocity of the m*Bt*CYP11A1-Q377A catalyzed reaction was 39% higher than that of the m*Bt*CYP11A1 mediated reaction (Fig. 7), explaining the improved activity of this mutant enzyme.

4. Discussion

Since the CYP11A1-catalyzed cholesterol side chain cleavage reaction plays a central role in sterol biosynthesis, a wealth of efforts have been made on biochemical characterization, structural elucidation of the enzyme-substrate complex, and catalytic mechanism [13,38,43,64–67]. However, there are very few reports on CYP11A1 protein engineering for activity improvement likely due to the high conservation

of this group of P450 enzymes and challenges in heterologous expression and biochemical characterization of these membrane-associated proteins. Thus, it is of great significance to explore natural CYP11A1 resources and engineer CYP11A1 to achieve better catalytic performance for potential industrial application.

Aiming to explore more natural CYP11A1s with better catalytic efficiencies, we successfully *in vitro* characterized four CYP11A1s in this study. Among the four CYP11A1 enzymes, the enzymatic properties of m*Ch*CYP11A1 and m*Ss*CYP11A1 were biochemically determined for the first time. Substrate specificity experiments showed that the four purified CYP11A1s could catalyze the C20-C22 bond cleavage reaction of five sterol substrates. These results indicate that these CYP11A1s have enough space to accommodate different substituent groups at the C17 position. Nonetheless, the bulkier is the C17 group, the lower is activity, which is consistent with the observation that the deep end space of CYP11A1s is narrow [13,43]. Moreover, further docking analysis indicated that the distance from C22 of 7-dehydrocholesterol to the heme-iron reactive center is the shortest among those of the five studied substrates, which at least partially explains the substrate preference of CYP11A1 for 7-dehydrocholesterol. By contrast, the distance from C22 of β-sitosterol to the heme-iron is the longest, which is attributed to steric hindrance caused by the volume increase of the side chain, thus leading to the lowest activity towards β-sitosterol.

For a multicomponent P450 system, it is pivotal to enhance the electron transfer efficiency through RP selection or engineering to enhance the P450′s catalytic activity [15]. Through RP mining and cross-combination screening, m*Ss*Adx/m*Ch*AdR were determined as the optimal RPs for m*Hs*CYP11A1, which provides a useful reference for the RPs selection for other mitochondrial P450s. Owing to the electron shuttle role of Adx in the electron transport pathway, the currently available crystal structure of the artificial CYP11A1-Adx fusion [13] may not clearly explain the natural interaction mechanism between CYP11A1 and Adx; thus, more efforts are required for further optimization of the CYP11A1-Adx interaction.

The catalytic mechanism of CYP11A1 has already been resolved: the three-step processive oxidation (Fig. 1) relies on the back-and-forth swing of the side chain of the substrate, which makes the whole catalytic process quite delicate and subtle. Therefore, it is very difficult to perform (semi-)rational engineering for the highly conserved active sites of CYP11A1. As demonstrated by this study, the alanine scanning of the active pocket did not result in any mutant with improved activity. On the contrary, the expression and activity of many mutants decreased to a large extent, indicating that the plasticity of the substrate binding pocket is poor. This pocket might have "perfectly" matched for the substrate during the long history of natural evolution in order to complete the housekeeping and catalytically challenging functionality of cleaving the side chain of cholesterol.

Directed evolution has been proved as an effective strategy for enzyme activity improvement [68–72]. However, there is no report on directed evolution of any CYP11A1s perhaps due to unavailability of a high-throughput screening method. Thus, despite lack of success of our semi-rational mutagenesis for the active site residues of m*Hs*CYP11A1, we performed alanine scanning for the substrate entrance channel residues because it has been well known that the amino acids at the substrate entrance channel are crucial for enzyme activities [58,59,73]. Supporting this, m*Bt*CYP11A1-Q377A with a widened substrate entrance channel turned out to be the first CYP11A1 mutant showing a higher activity than the corresponding wild type enzyme. Thus, we suggest that the future semi-rational mutagenesis should be more focused on the non-active site residues of CYP11A1s. Furthermore, according to the previous kinetic study, the dissociation of Adx and CYP11A1 is the rate-limiting step in the whole catalytic process [74]. Therefore, the amino acid residues involved in the Adx-CYP11A1 interaction could be potential sites for (semi-)rational mutagenesis, especially considering that similar successes have been achieved in other P450 systems [58,59,73]. However, caution should be exercised in Adx-CYP11A1 interface engineering because CYP11A1 and Adx might have co-evolved for millions of years, as the human CYP11A1 only showed none or poor activity when partnered with RhFRED or Fdx1499/FdR0978 (Fig. S9), which are widely accepted RPs by other P450 enzymes [44].

5. Conclusions

In conclusion, we biochemically characterized two new CYP11A1s with cholesterol side-chain cleavage function *in vitro*, expanding the toolbox of this kind of valuable biocatalysts. Moreover, one mutant (m*Bt*CYP11A1-Q377A) with improved activity was obtained, which we envision will become a new starting point for the future enzyme engineering of CYP11A1s. Hopefully, an industrially relevant CYP11A1 variant can be eventually engineered, thereby benefiting the total biosynthesis of steroid drugs.

Funding

This work was financially supported by the National Natural Science Foundation of China (32025001 and 31872729) and the Tianjin Synthetic Biotechnology Innovation Capability Improvement Action (TSBICIP-KJGG-001–12).

CRediT authorship contribution statement

Ruxin Liu and Shengying Li conceived this research. Ruxin Liu performed the majority of experiments. Yunjun Pan, Ning Wang, and Dandan Tang helped in different experiments such as protein expression and purification, and molecular docking. Ruxin Liu, Vlada B. Urlacher, and Shengying Li analyzed experimental results. Ruxin Liu, Vlada B. Urlacher, and Shengying Li wrote the manuscript. All authors read and approved the final manuscript.

Declaration of Competing Interest

The authors declare that they have no competing interests.

Data availability

Data will be made available on request.

Acknowledgements

We thank Professor Rita Bernhardt from Saarland University for providing us with the expression plasmids for bovine-derived Adx (4–108 aa) and AdR. We thank Xiangmei Ren, Jingyao Qu, Jing Zhu, and Zhifeng Li of the Core Facilities for Life and Environmental Sciences, State Key Laboratory of Microbial Technology at Shandong University for their help in ultra-high speed centrifugation and LC-MS analyses.

Appendix A. Supporting information

Supplementary data associated with this article can be found in the online version at doi:10.1016/j.jsbmb.2023.106268.

References

[1] P. Fernandes, A. Cruz, B. Angelova, H. Pinheiro, J. Cabral, Microbial conversion of steroid compounds: recent developments, Enzym. Microb. Technol. 32 (6) (2003) 688–705.

[2] L. Xiong, H. Liu, M. Zhao, Y. Liu, L. Song, Z. Xie, et al., Enhancing the bioconversion of phytosterols to steroidal intermediates by the deficiency of *kasB* in the cell wall synthesis of *Mycobacterium neoaurum*, Microb. Cell. Fact. 19 (1) (2020) 1–11.

[3] H. Peng, Y. Wang, K. Jiang, X. Chen, W. Zhang, Y. Zhang, et al., A dual role reductase from phytosterols catabolism enables the efficient production of valuable steroid precursors, Angew. Chem. Int. Ed. 133 (10) (2021) 5474–5480.

[4] M.V. Donova, O.V. Egorova, Microbial steroid transformations: current state and prospects, Appl. Microbiol. Biotechnol. 94 (6) (2012) 1423–1447.
[5] R.E. Marker, J. Krueger, Sterols. CXII. Sapogenins. XLI. The preparation of trillin and its conversion to progesterone, J. Am. Chem. Soc. 62 (12) (1940) 3349–3350.
[6] T. Wriessnegger, H. Pichler, Yeast metabolic engineering–targeting sterol metabolism and terpenoid formation, Prog. Lipid Res. 52 (3) (2013) 277–293.
[7] C. Duport, R. Spagnoli, E. Degryse, D. Pompon, Self-sufficient biosynthesis of pregnenolone and progesterone in engineered yeast, Nat. Biotechnol. 16 (2) (1998) 186–189.
[8] J. Chen, F. Fan, G. Qu, J. Tang, Y. Xi, C. Bi, et al., Identification of *Absidia orchidis* steroid 11β-hydroxylation system and its application in engineering *Saccharomyces cerevisiae* for one-step biotransformation to produce hydrocortisone, Metab. Eng. 57 (2020) 31–42.
[9] F.M. Szczebara, C. Chandelier, C. Villeret, A. Masurel, S. Bourot, C. Duport, et al., Total biosynthesis of hydrocortisone from a simple carbon source in yeast, Nat. Biotechnol. 21 (2) (2003) 143–149.
[10] R.J. Auchus, W.L. Miller, P450 enzymes in steroid processing, in: P. Ortiz de Montellano (Ed.), Cytochrome P450, Springer-Publishing Inc., Switzerland, 2015, pp. 851–879.
[11] C. Brocard-Masson, I. Bonnin, B. Dumas, Process for preparing genetically transformed yeasts capable of producing a molecule of interest at a high titre, Google Patents (2018).
[12] W.L. Miller, R.J. Auchus, The molecular biology, biochemistry, and physiology of human steroidogenesis and its disorders, Endocr. Rev. 32 (1) (2011) 81–151.
[13] N. Strushkevich, F. MacKenzie, T. Cherkesova, I. Grabovec, S. Usanov, H.W. Park, Structural basis for pregnenolone biosynthesis by the mitochondrial monooxygenase system, Proc. Natl. Acad. Sci. 108 (25) (2011) 10139–10143.
[14] H.K. Ghayee, R.J. Auchus, Basic concepts and recent developments in human steroid hormone biosynthesis, Rev. Endocr. Metab. Disord. 8 (4) (2007) 289–300.
[15] S. Li, L. Du, R. Bernhardt, Redox partners: function modulators of bacterial P450 enzymes, Trends Microbiol 28 (6) (2020) 445–454.
[16] P. Durairaj, S. Li, Functional expression and regulation of eukaryotic cytochrome P450 enzymes in surrogate microbial cell factories, Eng. Microb. 2 (1) (2022) 100011–100018.
[17] R. Zhang, Y. Zhang, Y. Wang, M. Yao, J. Zhang, H. Liu, et al., Pregnenolone overproduction in *Yarrowia lipolytica* by integrative components pairing of the cytochrome P450scc system, ACS Synth. Biol. 8 (12) (2019) 2666–2678.
[18] V.S. Efimova, L.V. Isaeva, M.A. Rubtsov, L.A. Novikova, Analysis of *in vivo* activity of the bovine cholesterol hydroxylase/lyase system proteins expressed in *Escherichia coli*, Mol. Biotechnol. 61 (4) (2019) 261–273.
[19] D.S. Makeeva, D.V. Dovbnya, M.V. Donova, L.A. Novikova, Functional reconstruction of bovine P450scc steroidogenic system in *Escherichia coli*, Am. J. Mol. Biol. 03 (04) (2013) 173–182.
[20] T. Shashkova, V. Luzikov, L. Novikova, Coexpression of all constituents of the cholesterol hydroxylase/lyase system in *Escherichia coli* cells, Biochem. (Mosc.) 71 (7) (2006) 810–814.
[21] H. Du, W. Xiao, Y. Wang, X. Zhou, Y. Zhang, D. Liu, et al., Engineering *Yarrowia lipolytica* for campesterol overproduction, PLoS One 11 (1) (2016), e0146773.
[22] R.C. Edgar, MUSCLE: multiple sequence alignment with high accuracy and high throughput, Nucleic Acids Res 32 (5) (2004) 1792–1797.
[23] I. Letunic, P. Bork, Interactive Tree Of Life (iTOL) v4: recent updates and new developments, Nucleic Acids Res 47 (W1) (2019) W256–W259.
[24] H.J. Barnes, M.P. Arlotto, M.R. Waterman, Expression and enzymatic activity of recombinant cytochrome P450 17 alpha-hydroxylase in *Escherichia coli*, Proc. Natl. Acad. Sci. 88 (13) (1991) 5597–5601.
[25] H. Uhlmann, R. Kraft, R. Bernhardt, C-terminal region of adrenodoxin affects its structural integrity and determines differences in its electron transfer function to cytochrome P-450, J. Biol. Chem. 269 (36) (1994) 22557–22564.
[26] S.N. Ho, H.D. Hunt, R.M. Horton, J.K. Pullen, L.R. Pease, Site-directed mutagenesis by overlap extension using the polymerase chain reaction, Gene 77 (1) (1989) 51–59.
[27] M. Hayer-Hartl, A. Bracher, F.U. Hartl, The GroEL–GroES chaperonin machine: a nano-cage for protein folding, Trends Biochem. Sci. 41 (1) (2016) 62–76.
[28] Y. Jiang, Z. Li, C. Wang, Y.J. Zhou, H. Xu, S. Li, Biochemical characterization of three new α-olefin-producing P450 fatty acid decarboxylases with a halophilic property, Biotechnol. Biofuels 12 (1) (2019) 1–14.
[29] T. Omufca, R. Sato, The carbon monoxide-binding pigment of liver microsomes, J. Biol. Chem. 239 (7) (1964) 2370–2378.
[30] J.J. Huang, T. Kimura, Adrenal steroid hydroxylases. Oxidation-reduction properties of adrenal iron-sulfur protein (adrenodoxin), Biochemistry 12 (3) (1973) 406–409.
[31] J. Chu, T. Kimura, Studies on adrenal steroid hydroxylases: molecular and catalytic properties of adrenodoxin reductase (a flavoprotein), J. Biol. Chem. 248 (6) (1973) 2089–2094.
[32] A. Waterhouse, M. Bertoni, S. Bienert, G. Studer, G. Tauriello, R. Gumienny, et al., SWISS-MODEL: homology modelling of protein structures and complexes, Nucleic Acids Res 46 (W1) (2018) W296–W303.
[33] G.M. Morris, R. Huey, W. Lindstrom, M.F. Sanner, R.K. Belew, D.S. Goodsell, et al., AutoDock4 and AutoDockTools4: Automated docking with selective receptor flexibility, J. Comput. Chem. 30 (16) (2009) 2785–2791.
[34] M. Masuo, D. Carmenza, I. Nobuo, S. Mikio, Substrate specificity of adrenocortical cytochrome P-450scc—I. Effect of structural modification of cholesterol side-chain on pregnenolone production, J. Steroid Biochem. 13 (5) (1980) 545–550.
[35] M. Masuo, D. Carmenza, T. Kumiko, I. Nobuo, S. Mikio, Substrate specificity of adrenocortical cytochrome P-450scc—II. Effect of structural modification of cholesterol A/B ring on their side chain cleavage reaction, J. Steroid Biochem. 16 (1) (1982) 101–105.
[36] M. Morisaki, M. Shikita, N. Ikekawa, [20] Side-chain cleavage of cholesterol by gas chromatography-mass spectrometry in a selected ion monitoring mode, in: R. Wu, L. Grossman, K. Moldave (Eds.), Methods in Enzymology, Academic Press, New York, 1985, pp. 352–364.
[37] R.C. Tuckey, K.J. Cameron, Catalytic properties of cytochrome P-450scc purified from the human placenta: comparison to bovine cytochrome P450scc, Biochim. Biophys. Acta 1163 (2) (1993) 185–194.
[38] R.C. Tuckey, K.J. Cameron, Side-chain specificities of human and bovine cytochromes P450scc, Eur. J. Biochem. 217 (1) (1993) 209–215.
[39] R.C. Tuckey, J. Lawrence, K.J. Cameron, Side-chain cleavage of cholesterol esters by human cytochrome P450scc, J. Steroid Biochem. Mol. Biol. 58 (5–6) (1996) 605–610.
[40] G. Li, T. An, Y. Li, J. Yue, R. Huang, J. Huang, et al., Transcriptome analysis and identification of the cholesterol side chain cleavage enzyme *Bbg*CYP11A1 from *Bufo bufo gargarizans*, Front. Genet. 13 (2022) 828877–828889.
[41] P. Hartz, S.J. Strohmaier, B.M. EL-Gayar, A. Abdulmughni, M.C. Hutter, F. Hannemann, et al., Resurrection and characterization of ancestral CYP11A1 enzymes, FEBS J. 288 (22) (2021) 6510–6527.
[42] A. Luthra, I.G. Denisov, S.G. Sligar, Spectroscopic features of cytochrome P450 reaction intermediates, Arch. Biochem. Biophys. 507 (1) (2011) 26–35.
[43] N. Mast, A.J. Annalora, D.T. Lodowski, K. Palczewski, C.D. Stout, I.A. Pikuleva, Structural basis for three-step sequential catalysis by the cholesterol side chain cleavage enzyme CYP11A1, J. Biol. Chem. 286 (7) (2011) 5607–5613.
[44] F. Hannemann, A. Bichet, K.M. Ewen, R. Bernhardt, Cytochrome P450 systems—biological variations of electron transport chains, Biochim. Biophys. Acta 1770 (3) (2007) 330–344.
[45] W. Zhang, L. Du, F. Li, X. Zhang, Z. Qu, L. Han, et al., Mechanistic insights into interactions between bacterial class I P450 enzymes and redox partners, ACS Catal. 8 (11) (2018) 9992–10003.
[46] Z. Li, Y. Jiang, F.P. Guengerich, L. Ma, S. Li, W. Zhang, Engineering cytochrome P450 enzyme systems for biomedical and biotechnological applications, J. Biol. Chem. 295 (3) (2020) 833–849.
[47] Y. Khatri, F. Hannemann, K.M. Ewen, D. Pistorius, O. Perlova, N. Kagawa, et al., The CYPome of *Sorangium cellulosum So ce56* and identification of CYP109D1 as a new fatty acid hydroxylase, Chem. Biol. 17 (12) (2010) 1295–1305.
[48] K.M. Ewen, F. Hannemann, S. Iametti, A. Morleo, R. Bernhardt, Functional characterization of Fdx1: evidence for an evolutionary relationship between P450-type and ISC-type ferredoxins, J. Mol. Biol. 413 (5) (2011) 940–951.
[49] X. Liu, F. Li, T. Sun, J. Guo, X. Zhang, X. Zheng, et al., Three pairs of surrogate redox partners comparison for Class I cytochrome P450 enzyme activity reconstitution, Commun. Biol. 5 (1) (2022) 1–11.
[50] S. Li, L.M. Podust, D.H. Sherman, Engineering and analysis of a self-sufficient biosynthetic cytochrome P450 PikC fused to the RhFRED reductase domain, J. Am. Chem. Soc. 129 (43) (2007) 12940–12941.
[51] Y. Sun, L. Ma, D. Han, L. Du, F. Qi, W. Zhang, et al., *In vitro* reconstitution of the cyclosporine specific P450 hydroxylases using heterologous redox partner proteins, J. Ind. Microbiol. Biotechnol. 2 (44) (2016) 161–166.
[52] W. Zhang, Y. Liu, J. Yan, S. Cao, F. Bai, Y. Yang, et al., New reactions and products resulting from alternative interactions between the P450 enzyme and redox partners, J. Am. Chem. Soc. 136 (9) (2014) 3640–3646.
[53] Y. Sun, L. Ma, D. Han, L. Du, F. Qi, W. Zhang, et al., *In vitro* reconstitution of the cyclosporine specific P450 hydroxylases using heterologous redox partner proteins, J. Ind. Microbiol. Biotechnol. 44 (2) (2017) 161–166.
[54] A.V. Glyakina, N.I. Strizhov, M.V. Karpov, N.V. Dovidchenko, B.T. Matkarimov, L. V. Isaeva, et al., Ile351, Leu355 and Ile461 residues are essential for catalytic activity of bovine cytochrome P450scc (CYP11A1), Steroids 143 (2019) 80–90.
[55] I.A. Pikuleva, R.L. Mackman, N. Kagawa, M. Waterman, P.O. Demontellano, Active-site topology of bovine cholesterol side-chain cleavage cytochrome P450 (P450scc) and evidence for interaction of tyrosine 94 with the side chain of cholesterol, Arch. Biochem. Biophys. 322 (1) (1995) 189–197.
[56] P. Ghisellini, C. Paternolli, C. Nicolini, Site-directed mutations (Asp405Ile and Glu124Ile) in cytochrome P450scc: effect on adrenodoxin binding, J. Cell. Biochem 95 (4) (2005) 720–730.
[57] S. Janocha, A. Bichet, A. Zöllner, R. Bernhardt, Substitution of lysine with glutamic acid at position 193 in bovine CYP11A1 significantly affects protein oligomerization and solubility but not enzymatic activity, Biochim. Biophys. Acta 1814 (1) (2011) 126–131.
[58] G. Li, P. Yao, R. Gong, J. Li, P. Liu, R. Lonsdale, et al., Simultaneous engineering of an enzyme's entrance tunnel and active site: the case of monoamine oxidase MAO-N, Chem. Sci. 8 (5) (2017) 4093–4099.
[59] K. Prakinee, A. Phintha, S. Visitsatthawong, N. Lawan, J. Sucharitakul, C. Kantiwiriyawanitch, et al., Mechanism-guided tunnel engineering to increase the efficiency of a flavin-dependent halogenase, Nat. Catal. 5 (6) (2022) 534–544.
[60] Z. Bata, Z. Molnar, E. Madaras, B. Molnar, E. Santa-Bell, A. Varga, et al., Substrate tunnel engineering aided by X-ray crystallography and functional dynamics swaps the function of MIO-enzymes, ACS Catal. 11 (8) (2021) 4538–4549.
[61] X. Yang, L. Wu, A. Li, L. Ye, J. Zhou, H. Yu, The engineering of decameric d-fructose-6-phosphate aldolase A by combinatorial modulation of inter-and intra-subunit interactions, Chem. Commun. 56 (55) (2020) 7561–7564.
[62] S. Meng, R. An, Z. Li, U. Schwaneberg, Y. Ji, M.D. Davari, et al., Tunnel engineering for modulating the substrate preference in cytochrome $P450_{Bs\beta}$HI, Bioresour. Bioprocess 8 (1) (2021) 1–10.

[63] A. Mosa, J. Neunzig, A. Gerber, J. Zapp, F. Hannemann, P. Pilak, et al., 2β-and 16β-hydroxylase activity of CYP11A1 and direct stimulatory effect of estrogens on pregnenolone formation, J. Steroid Biochem. Mol. Biol. 150 (2015) 1–10.
[64] J.R. Arthur, H.A. Blair, G.S. Boyd, J. Mason, K. Suckling, Oxidation of cholesterol and cholesterol analogues by mitochondrial preparations of steroid-hormone-producing tissue, Biochem. J. 158 (1) (1976) 47–51.
[65] R. Davydov, A.A. Gilep, N.V. Strushkevich, S.A. Usanov, B.M. Hoffman, Compound I is the reactive intermediate in the first monooxygenation step during conversion of cholesterol to pregnenolone by cytochrome P450scc: EPR/ENDOR/cryoreduction/annealing studies, J. Am. Chem. Soc. 134 (41) (2012) 17149–17156.
[66] F.K. Yoshimoto, I.J. Jung, S. Goyal, E. Gonzalez, F.P. Guengerich, Isotope-labeling studies support the electrophilic Compound I iron active species, FeO^{3+}, for the carbon-carbon bond cleavage reaction of the cholesterol side-chain cleavage enzyme, cytochrome P450 11A1, J. Am. Chem. Soc. 138 (37) (2016) 12124–12141.
[67] H. Su, B. Wang, S. Shaik, Quantum-mechanical/molecular-mechanical studies of CYP11A1-catalyzed biosynthesis of pregnenolone from cholesterol reveal a C–C bond cleavage reaction that occurs by a Compound I-mediated electron transfer, J. Am. Chem. Soc. 141 (51) (2019) 20079–20088.
[68] P.A. Romero, F.H. Arnold, Exploring protein fitness landscapes by directed evolution, Nat. Rev. Mol. Cell Biol. 10 (12) (2009) 866–876.
[69] K. Chen, F.H. Arnold, Engineering new catalytic activities in enzymes, Nat. Catal. 3 (3) (2020) 203–213.
[70] H. Xu, W. Liang, L. Ning, Y. Jiang, W. Yang, C. Wang, et al., Directed evolution of P450 fatty acid decarboxylases via high-throughput screening towards improved catalytic activity, ChemCatChem 12 (1) (2020) 80–84.
[71] Y. Wang, P. Xue, M. Cao, T. Yu, S.T. Lane, H. Zhao, Directed evolution: methodologies and applications, Chem. Rev. 121 (20) (2021) 12384–12444.
[72] M.D. Lane, B. Seelig, Advances in the directed evolution of proteins, Curr. Opin. Chem. Biol. 22 (2014) 129–136.
[73] L. Ba, P. Li, H. Zhang, Y. Duan, Z. Lin, Semi-rational engineering of cytochrome P450sca-2 in a hybrid system for enhanced catalytic activity: insights into the important role of electron transfer, Biotechnol. Bioeng. 110 (11) (2013) 2815–2825.
[74] B. Schiffler, A. Zollner, R. Bernhardt, Stripping down the mitochondrial cholesterol hydroxylase system, a kinetics study, J. Biol. Chem. 279 (33) (2004) 34269–34276.